Luminescent Tetradentate Gold(III)-TADF Emitters: Microwave-Assisted Synthesis and High Performance OLEDs With EQEs Up To 25 % and Long Operational Lifetime

Dongling Zhou,[a] Wai-Pong To,[a] Glenna So Ming Tong,[a] Gang Cheng,[a,b] Lili Du,[a] David Lee Phillips,[a] and Chi-Ming Che*[a,b]

Abstract: Structurally robust tetradentate gold(III)-emitters have potent material applications but are rare and unprecedented for those displaying thermally activated delayed fluorescence (TADF). In this work, a novel synthetic route leading to the preparation of highly emissive, charge-neutral tetradentate [C^C^N^C] gold(III) complexes with 5-5-6 membered chelate rings has been developed through microwave-assisted C−H bond activation. These complexes show high thermal stability and with emission origin (^{3}IL, ^{3}ILCT and TADF) tuned by varying the substituents of the C^C^N^C ligand. With phenoxazine/diphenylamine substituent, we prepared the first tetradentate gold(III)-TADF emitters with emission quantum yields of up to 94 % and emission lifetimes of down to 0.62 μs in deoxygenated toluene. These tetradentate Au^{III}-TADF emitters showed good performance in vacuum-deposited OLEDs with maximum EQEs of up to 25 % and LT_{95} of up to 5280 h at 100 cd m^{-2}.

Introduction

Gold metal is appealing in the development of new generation of luminescent molecular materials due to strong gold-ligand bond that confers high thermal stability, large spin-orbit coupling (SOC) constant for harvesting triplet excitons, and much higher earth abundance than the other precious noble metals. Nonetheless, the practical applications of luminescent gold complexes remain in the "proof-of-concept" stage. Despite the extensive works on luminescent gold complexes over the past decade, examples of gold OLEDs with exemplary performance data close to that of the best iridium-OLEDs are very rare, and these rare examples were reported only in the past several years (EQEs of Au^{I} and Au^{III} OLEDs up to 27.5 % and 23.8 % respectively) by exploiting the TADF mechanism.[1] The mainstream design of luminescent Au^{III} complexes is the combined use of two or more ligands. As the stability of metal complexes could be improved by increasing the denticity of chelating ligands and metal-ligand bond strength, the use of rigid tetradentate ligands having C-donor atom(s) is conceived to endow high thermal stability to the complex and to restrict excited state structural distortion. While strongly luminescent tetradentate Pt^{II} and Pd^{II} emitters are well documented,[2] there is one literature report on non-porphyrin type charge-neutral tetradentate Au^{III} complexes prepared by an intramolecular cyclization between two ligands with tridentate alkynylgold(III) complexes as precursors, reported by Yam and co-workers.[3d] Nonetheless, it would be a formidable challenge to use this post-synthetic modification strategy for preparing structurally diverse tetradentate Au^{III} core structures. On the other hand, the radiative decay rate constants of phosphorescent Au^{III} complexes are usually small as the emissive excited states being mainly ligand localized, involve only minor metal parentage, which is detrimental in OLED applications due to large efficiency roll-off.[3] In this regard, OLEDs fabricated with Au^{I} and Au^{III}-TADF emitters (τ < 2 μs) have achieved small roll-off (< 10 %).[1a,b,e] A recent study suggested that improving the rigidity of emitters could suppress the structural deformation upon S_1–T_1 transformation thereby reducing the activation energy barrier for reverse intersystem crossing (RISC) and leading to efficient TADF.[4] It is thus conceived that Au^{III} complexes supported by trianionic tetradentate ligands and exhibiting efficient TADF at room temperature would be a way forward.

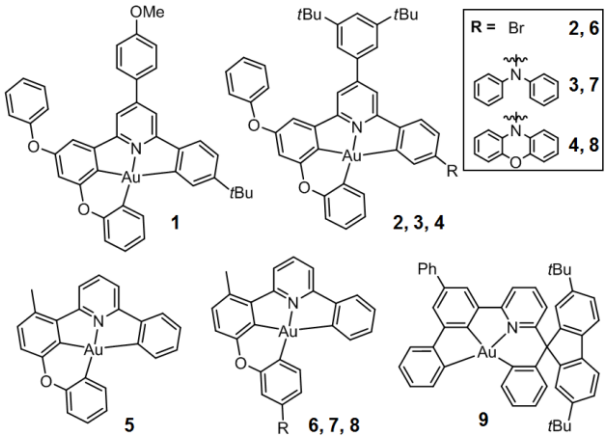

Figure 1. Chemical structures of **1**−**9**.

[a] D. Zhou, Dr. W.-P. To, Dr. G. S. M. Tong, Dr. G. Cheng, Dr. L. Du, Prof. Dr. D. L. Phillips, Prof. Dr. C.-M. Che
State Key Laboratory of Synthetic Chemistry, HKU-CAS Joint Laboratory on New Materials, Department of Chemistry, The University of Hong Kong
Pokfulam Road, Hong Kong SAR (China)
E-mail: cmche@hku.hk

[b] Dr. G. Cheng, Prof. Dr. C.-M. Che
HKU Shenzhen Institute of Research and Innovation
Shenzhen, Guangdong, 518053 (China)

Supporting information for this article is given via a link at the end of the document.

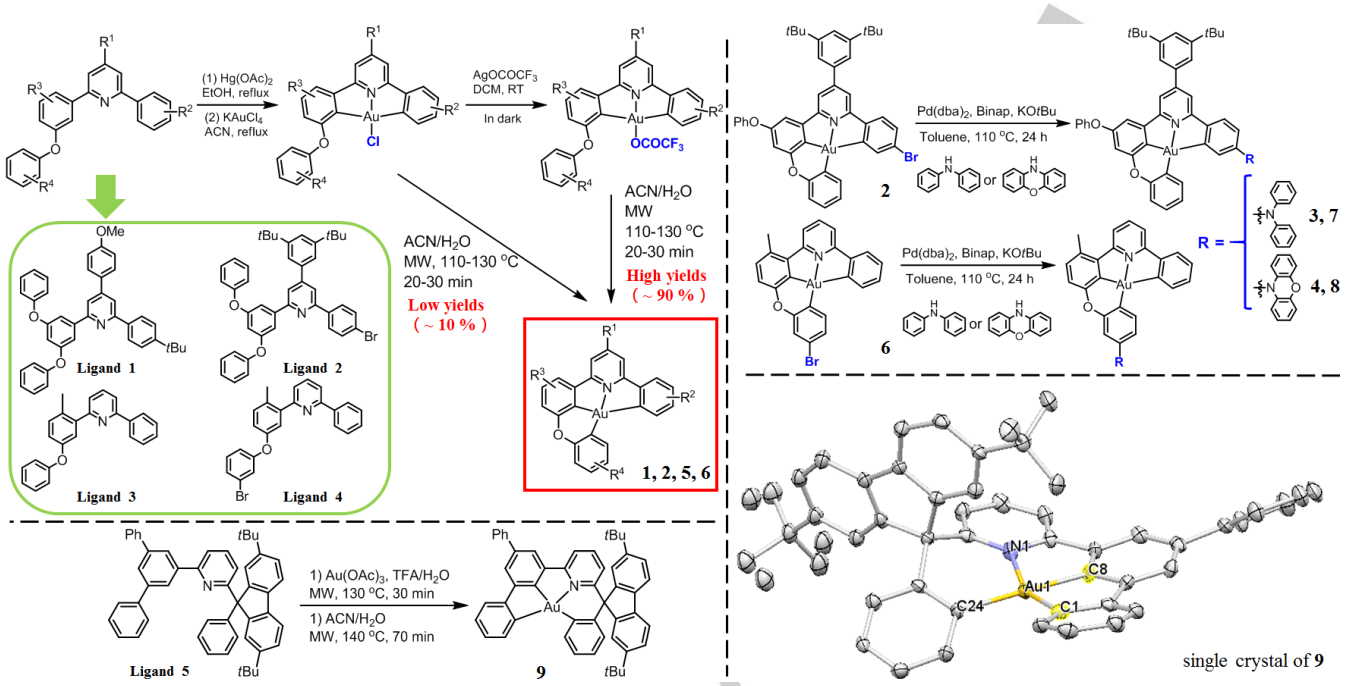

Figure 2. Synthetic scheme of Au^{III} complexes **1**–**9** and ORTEP drawing for **9** with omission of hydrogen atoms (thermal ellipsoids probability level: 30%).

Herein are described new synthetic routes for preparing tetradentate Au^{III} complexes supported by O-bridged/spiro-arranged C^C^N^C ligand scaffolds through microwave-induced C–H activation. This synthetic strategy has previously been used for the preparation of bidentate/tridentate Au^{III} complexes.[5] With judicious choice of substituent(s) on the ligand scaffold, the emission origin of these complexes could be tuned from long-lived ^{3}IL excited state to TADF from ILCT excited state. Stable, highly efficient tetradentate Au^{III}-TADF emitters with emission quantum yields (Φ) of up to a record-high 94 % and lifetimes (τ) down to 0.62 μs have been realized and applications of these emitters in OLEDs have also been explored.

Results

Synthesis and Characterization

In these complexes, 3,5-diphenoxyphenyl, 2-methyl-5-phenoxyphenyl and 3,5-diphenyl moieties were used to ensure the presence of a pendent phenyl/phenoxy ring which can coordinate to Au^{III} *trans* to the pyridine to form the C^C moiety. As shown in Figure 2, complexes **1**, **2**, **5** and **6** were prepared by using cyclometalated Au^{III} trifluoroacetate ($OCOCF_3^-$) as precursors in a 1:1 (v/v) mixture of ACN/H_2O in high yields (~90 %) under microwave heating at 110–130 °C. Cyclometalated Au^{III} chlorides could also be used, albeit with low yields (roughly 10 %). The desired product was not formed when cyclometalated Au^{III}-$OCOCF_3$ was refluxed in ACN/H_2O (1:1 v/v) for 24 hours, thus establishing the crucial role of microwave irradiation in the synthesis of tetradentate cyclometalated Au^{III} complexes. Cyclometalated Au^{III} chlorides supported by ligands with amino-substituted moieties (diphenylamine or phenoxazine)/spiro-fluorene are difficult to be obtained by traditional methods such as transmetalation from organomercury compounds or direct auration from L-$AuCl_3$. Therefore, complexes **3**, **4**, **7** and **8** were prepared by Pd-catalyzed reactions between **2** or **6** and corresponding amines in moderate yields (40–47 %). Complex **9** was obtained in 36 % yield via mercury-free direct auration by using $Au(OAc)_3$ in two consecutive microwave-assisted reactions. Microwave-assisted direct auration with $KAuCl_4$ or $Au(OAc)_3$ failed to give **1**, **2**, **5** and **6**.

The crystal structure of **9** is depicted in Figure 2 and that of **1** and **5** are depicted in Figure S3-S4. The Au^{III} atoms adopt distort square-planar geometries with C–Au–C and C–Au–N angles of 157.98–161.31° and 170.47–173.40°, respectively. The Au–C and Au–N bond distances are 1.950–2.028 Å and 2.028–2.115 Å, respectively. Except for the moieties that are not coordinated to the metal ion (4-methoxyphenyl and phenoxyphenyl), the Au(C^C^N^C) unit of **1** is nearly coplanar. Unlike **1**, the phenoxyphenyl moiety of **5** is slightly out-of-plane, making a torsion angle with the Au(C^N^C) plane of 15.13°. For **9**, spiro-fluorene moiety exhibits out-of-plane bending conformation

Table 1. Photophysical and electrochemical data of **1**–**9**.

Complex	Absorption	Emission[b]		*E* (V vs. SCE)[e]	
	λ_{abs} [nm] (ε [×10^3 mol^{-1} dm^3 cm^{-1}])[a]	In toluene λ_{em} [nm] (Φ; τ [μs]; k_r [10^3 s^{-1}])	In thin films λ_{em} [nm] (Φ; τ [μs]; k_r [10^3 s^{-1}])	Oxidation (E_{pa})	1st Reduction ($E_{1/2}$)
1	317(15.16), 331(14.20), 381(5.21)	495, 526, 565 (0.54; 93.1; 5.8)	492, 523, 560[c] (0.20; 43.8; 4.57)	––	−1.45
2	315(12.75), 381(5.60)	498, 526, 567 (0.40; 77.1; 5.2)	490, 522, 562[c] (0.04; 90.1; 0.44)	––	−1.38[h]
3	302(38.73), 382(29.02), 456(br, 12.29)	524, 550 (0.77; 94.3; 8.2)	550[c] (0.47; 56.8; 8.27)	1.01[g]	−1.43
4	311(37.04), 380(13.35), 465(br, 2.07)	612 (0.47; 0.62; 758)	568[d] (0.89; 1.69; 527)	0.75[f]	−1.36
5	304(8.09), 379(5.89), 394(5.00)	493, 521 (0.28; 225; 1.2)	489, 519, 555[c] (0.06; 147; 0.41)	––	−1.50
6	300(8.53), 378(5.70), 390(4.75)	485, 518, 552 (0.26; 152; 1.7)	486, 518, 555[c] (0.06; 90.4; 0.66)	––	−1.47
7	301(37.06), 380(13.26), 393(12.32), 424(br, 6.68)	533 (0.94; 1.61; 584)	520[d] (0.82; 2.08; 394)	1.04	−1.51
8	303(19.28), 325(13.88), 378(10.98), 391(9.21), 422(br, 1.16)	580 (0.74; 0.79; 937)	568[d] (0.71; 2.54; 280)	0.77[f]	−1.48
9	305(22.07), 337(9.35), 395(2.61)	480, 513, 557 (0.003; 1.04; 2.88)	482, 515, 552[c] (0.06, 36.01, 1.67)	––	−1.59

[a] In degassed toluene (2 × 10^{-5} mol dm^{-3}) at room temperature. "br" stands for broad. [b] Emission quantum yields were measured with Hamamatsu C11347 Quantaurus-QY Absolute PL quantum yields measurement system. [c] PMMA thin film samples (with 4 wt% of Au^{III} complex). [d] TCTA thin film samples (with 16 wt% of **4**, 8 wt% of **7** and 4 wt% of **8**). [e] E_{pa} refers to anodic peak potential for the irreversible oxidation waves. E_{pc} refers to cathodic peak potential for the irreversible reduction waves. $E_{1/2}$ = (E_{pa} + E_{pc})/2. [f] Reversible oxidation couples. [g] Quasi-reversible oxidation couples. [h] Irreversible reduction waves.

owing to steric strain, showing a dihedral angle with the C^C^N^C ligand plane of ~74.5°. Intermolecular π-π stacking between C^C^N^C ligands exists in **1** and **5** with interplanar distances of ~3.4 Å.

The electrochemical properties of **1**−**9** in DMF were investigated (Table 1). Except for **2** which displays an irreversible reduction wave at -1.38 V, these complexes show one reversible reduction couple at -1.36 to -1.59 V. These reduction peaks are assigned to the reduction of C^C^N^C ligands. Complexes **4** and **8** having a phenoxazine (PXZ) as a donor unit display a reversible oxidation couple at 0.75–0.77 V, while complexes **3** and **7** bearing a diphenylamine (DPA) show a quasi-reversible couple / irreversible wave at 1.01–1.04 V. These oxidation peaks are attributable to the oxidation of the amino-substituted moieties.

Spectroscopic and Photophysical Properties

The UV-visible absorption and emission spectral data of **1**−**9** are given in Table 1 and S8. In toluene, complexes **1**−**9** show intense absorption bands [ε = (1−4) ×10^4 dm^3 mol^{-1} cm^{-1}] at ca. 300−330 nm and moderately intense absorption bands [ε = (3–29) ×10^3 dm^3 mol^{-1} cm^{-1}] at ca. 340−400 nm, both of which are attributed to metal-perturbed intraligand π to π* transitions (^{1}IL) of the [C^C^N^C] ligand. Lower-energy absorption bands/tails are observed in amino-substituted complexes, assignable to intraligand charge transfer transitions (^{1}ILCT) from π(PXZ/DPA) to π*(C^C^N^C). More intense CT absorption is observed in the complexes having DPA [ε = (7–12) ×10^3 dm^3 mol^{-1} cm^{-1}] than the ones with PXZ [ε = (1–2) ×10^3 dm^3 mol^{-1} cm^{-1}]. DFT calculations revealed that this lowest energy absorption band is derived from the HOMO → LUMO transition with the HOMO mainly localized on the PXZ / TPA (TPA = triphenylamine) moieties whereas the LUMO is dominantly localized on the C^N^C part of the C^C^N^C ligand (Table S10). As the PXZ moiety in both complexes **4** and **8** is disposed nearly perpendicular to the C^N^C plane, the overlap between the HOMO and LUMO orbitals is small, leading to a small oscillator strength for the PXZ-bearing complexes (f = 0.0002–0.0003). On the other hand, one of the phenyl substituents in the TPA moiety of complexes **3** and **7** is nearly coplanar with the C^N^C plane, resulting in better overlap between the HOMO and LUMO and thus larger oscillator strength (f = 0.1491–0.2383).

In deoxygenated toluene, complexes **1**−**9** display blue-green to red photoluminescence at room temperature with three different types of emission profiles. Complexes **1**, **2**, **5**, **6** and **9** display blue-green to green emission featuring vibronically structured emission bands with Φ and τ of up to 0.54 and 225 μs, respectively; their radiative decay rate constants (k_r) range from 1.2 × 10^3 to 5.8 × 10^3 s^{-1}. Given the large Stokes shifts (4500−6000 cm^{-1}), vibronically structured emission bands and similar k_r of moderate magnitudes (~10^3 s^{-1}), the emissions of **1**,

2, **5**, **6** and **9** are assigned to ^{3}π-π*[C^C^N^C] phosphorescence. Complexes **3**, **4**, **7** and **8** which possess amino-substituent on the ligand display broad emission bands with emission color ranging from yellowish green to red; in particular, the Φ reaches a record-high value of 0.94 among Au(III) metal complexes. In aerated toluene, the emissions of **3**, **4**, **7** and **8** are strongly quenched by more than >90 %, suggesting that their triplet excited states contribute to the observed emission.

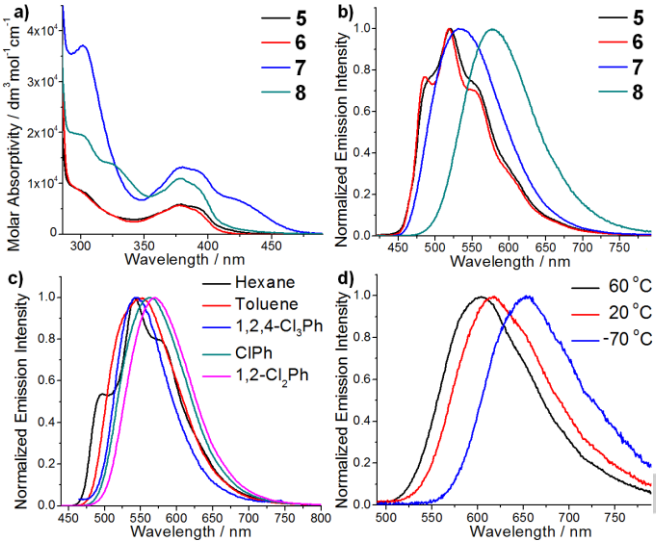

Figure 3. a) and b) Absorption and emission spectra of **5**−**8** in degassed toluene (conc. 2×10^{-5} mol dm^{-3}) at room temperature; c) emission spectra of **3** in different solvents; d) emission spectra of **4** in degassed toluene at different temperatures.

Solvent Effect and TADF Emission

To further elucidate the nature of the emissive excited state of complexes **3**, **4**, **7**, and **8**, the solvent effect on their emission properties was examined. The emissions of **3**, **4**, **7** and **8** display significant positive solvatochromism with the emission λ_{max} red-shifted by 638−2113 cm^{-1}. The Lippert–Mataga plots are linear with large positive slopes of 8490–12630 cm^{-1} (Figure S8), indicative of a large change in dipole moment upon attaining the emissive excited state and revealing the strong charge-transfer character of these emissive excited states. Although the emission profiles of these complexes vary from vibronically-structured in hexane to broad and featureless in polar solvents, the linear Lippert-Mataga plot with no inflection suggests a simple evolution from one state to another. As the emission of complex **3** is relatively long-lived (τ = 94 μs) with moderate k_r (8.16×10^3 s^{-1}), the emission of **3** is probably derived from ^{3}ILCT [π(diphenylamine) to π*(C^C^N^C)] mixed with ^{3}IL π-π*[C^C^N^C] excited state. [3d] Complexes **4**, **7** and **8**, on the other hand, being short-lived (τ < 2 μs) with large k_r (~10^5−10^6 s^{-1}) display emission behaviors that are similar to the reported Au^{III}-TADF complexes.[1a,e] Thus, the emission of **4**, **7**, and **8** likely involves TADF.

To further elucidate the nature of the emissive excited states of **4**, **7** and **8**, their emission in oxygen-free toluene was measured at different temperatures (Figure S9 and Table S9). It is observed that when the temperature was lowered from 20 to −70 °C, k_r of all three complexes decreased with temperature, giving support that the emission mechanism is thermally activated and is thus consistent with the assignment of emission origins involving TADF. When the temperature was raised from 20 to 60 °C, the k_r of **7** and **8** dropped while that of **3** increased slightly; this indicates that the energy barrier in the thermally activated process is not a constant and may vary with temperature. It should be noted that the charge separation in a charge transfer excited state depends on the polarity of the solvent, which in turn affects the size of exchange interaction and hence, the ΔE_{ST}.[6] Since the polarity of toluene decreases with increasing temperature,[7] it is possible that such increase in temperature would reduce the charge separation in the ^{1,3}CT excited states[6] and hence, ΔE_{ST} increases. That is, as the temperature increases from 20 to 60 °C, ΔE_{ST} increases, thus decreasing the contributions from the TADF emission mechanism, and hence, k_r decreases.

Time-Resolved Absorption Spectroscopy

The excited state nature and dynamics of the complexes have been investigated by nano/femtosecond time resolved spectroscopy. Nanosecond time-resolved absorption difference (ns-TA) spectra of **1**−**9** were obtained with 355 nm laser pulse excitation (Figure S10). Complexes **1** and **2** (**5** and **6**), which are supported by similar C^C^N^C ligand scaffold and exhibit ^{3}IL phosphorescence, show similar ns-TA spectra, revealing that their emissive excited states share similar electronic nature. For **3**, **4**, **7**, and **8**, their TA absorption profiles are unique to each complex, indicating that they are not derived from the same excited state. This is consistent with their steady-state emission characteristics where the emissions of **3**, **4, 7,** and **8** are charge transfer in nature, which depends on the donor and acceptor identities. Although complex **9** also displays ^{3}IL emission, the ligand scaffold is different from that of **1, 2**, **5,** and **6**; hence the ns-TA profiles of **9** are also different from those of **1, 2**, **5,** and **6**.

Femtosecond time-resolved absorption (fs-TA) spectra of these complexes have been recorded except for **2**, **6** and **9** which show poor solubility in toluene at a high concentration (Figure S11). Complexes **1**, **3**−**5**, **7** and **8** show striking differences between their fs-TA spectra, revealing different electronic configurations of their excited states. Clear spectral transformation with sets of isosbestic points can be observed in the early absorption spectra from the initial precursor state to the developed successor state. Since the successor state observed in fs-TA is consistent with the corresponding ns-TA spectra (Figure S10), the spectral transformation can be reasonably assigned as ISC from S_n to T_1. In the late-time fs-TA spectra of

these complexes, an ultrafast process is found in the triplet excited state, attributable to solvent reorientation or vibrational

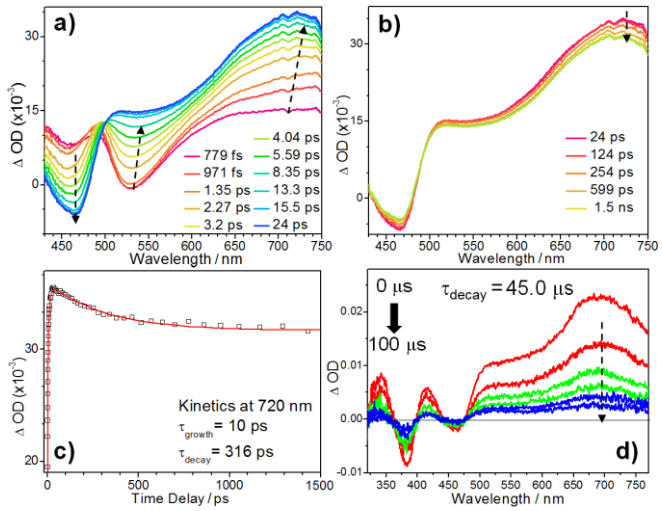

Figure 4. a) The early spectral conversion and b) the late-time process of fs-TA spectrum of **3** in toluene; c) kinetic study of fs-TA of **3**; d) ns-TA spectrum of **3** in toluene.

cooling. Kinetic study at selected wavelengths of these fs-TA spectra reveals that there are two components in the spectral evolution, defined as τ_{growth} and τ_{decay}, with the fast component τ_{growth} correlating with the process of ISC. Except for **8** with relatively long τ_{growth} of 56 ps, the intersystem crossing time constants (τ_{ISC} = 0.4−10 ps) of these compounds are comparable to those of the reported Au^{III} complexes with τ_{ISC} of ~0.2−13 ps.[8] The k_{ISC} of these tetradentate Au^{III} complexes can be estimated according to the formula of $k_{ISC} = 1/\tau_{growth}$ and also given herein (Table 2). The relatively long τ_{decay} of 45−2436 ps in Figure S11 are thus ascribed to the aforementioned ultrafast process in the triplet excited state.

Table 2. Estimated k_{ISC} of tetradentate Au^{III} complexes.

Complex	**1**	**3**	**4**	**5**	**7**	**8**
τ_{growth} [ps]	0.4	10	1.7	0.4	9.3	56
k_{ISC} [$\times 10^{11}$ s^{-1}]	25	1.0	5.9	25	1.1	0.18

DFT/TDDFT Calculations

It is observed from **3** and **7** that the position of the DPA in the complex has a strong impact on their k_r (k_r of **7** is of the order 10^5 s^{-1} while that of **3** is ~8 × 10^3 s^{-1} in both solution and film states). To understand the factor(s) that lead to the very different k_r in **3** and **7**, DFT/TDDFT calculations have been performed on these two complexes. Both the first singlet (S_1) and triplet (T_1) excited states display charge transfer (CT) character, as reflected from the charge density difference (CDD) maps and the associated natural transition orbitals (NTO) depicted in Figure S12 and Figure 5 respectively. The NTO pair, highest occupied NTO (HONTO) and the lowest unoccupied NTO (LUNTO), contributes dominantly to the S_1 and T_1 excited states (eigenvalue ν > 0.97). For both complexes, the HONTO is localized mainly on the DPA moiety and the phenyl ring the DPA directly attached to while the LUNTO is mainly on the C^N^C part of the C^C^N^C ligand. Of particular note is that, in complex **3**, the DPA moiety is directly attached to the phenyl ring of the C^N^C part of the C^C^N^C ligand; as such, the HONTO-LUNTO overlap is larger in **3** than in **7** (Table S12) and the energy gap between the S_1 and T_1 excited states (ΔE_{ST} = $E(S_1)$–$E(T_1)$) of **3** is much larger than that of **7** (ΔE_{ST} = 2466 and

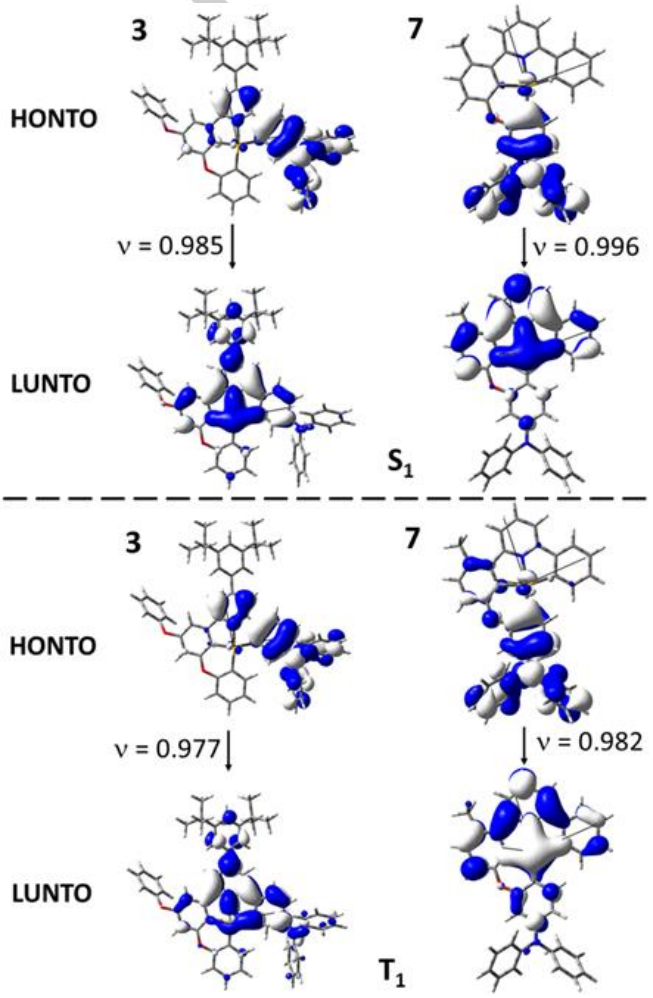

Figure 5. NTO pairs for the S_1 (top) and T_1 (bottom) excited states of complexes **3** (left) and **7** (right). Isovalue = 0.02 a.u.

Table 3. Key performances of OLEDs based on **4** with different doping concentrations.

Conc. [wt%]	Luminance [cd m^{-2}][a]	Current efficiency [cd A^{-1}]		Power efficiency [lm W^{-1}]		EQE [%][b]		CIE [(x, y)][c]
		Max.	at 1000 cd m^{-2}	Max.	at 1000 cd m^{-2}	Max.	at 1000 cd m^{-2}	
4	7300	65.59	53.23	91.98	49.18	20.84	16.79	0.38, 0.56
8	16500	70.82	64.44	81.73	62.38	22.72	21.21	0.40, 0.55
16	22700	77.78	67.48	94.00	63.72	25.03	22.01	0.43, 0.54

[a] At a driving voltage of 7 V. [b] External quantum efficiency. [c] CIE coordinates at 1000 cd m^{-2}.

686 cm^{-1} for complexes **3** and **7** respectively). The much smaller ΔE_{ST} in **7** suggests more favorable ISC and RISC; in turn, the much faster k_r in **7** is thus likely to be due to more efficient TADF.

To give further theoretical support that the much faster k_r in complex **7**, as compared with complex **3**, is due to more efficient TADF in the former, their k_r values have also been computed based on optimized excited state geometries. The character of the optimized S_1 and T_1 excited states are also CT in nature and are similar to those at their respective optimized S_0 geometries (Figure S13–S14). At the optimized ^{3}CT geometries, ΔE_{ST} remains large for **3** (ΔE_{ST} ~ 2800 cm^{-1}). The corresponding calculated $k_r^P(^3CT \rightarrow S_0)$ is 1.06 × 10^3 s^{-1} and the average k_r ($k_{r,avg}$), which takes into account both phosphorescence and TADF assuming Boltzmann statistics, slightly increases to 1.10 × 10^3 s^{-1} (assuming that the ^{1,3}CT excited states are in fast thermal equilibrium). As the experimental k_r is also of the order 10^3 s^{-1}, the emission of **3** is consistent with dominant $^3CT \rightarrow S_0$ phosphorescence. On the other hand, for **7**, at the optimized ^{3}CT geometry, ΔE_{ST} increases to 1700 cm^{-1}, possibly due to the shortened Au–N(pyridine) and C(phenyl)–N(DPA) distances, leading to stronger HONTO-LUNTO overlap (Table S13). The corresponding calculated $k_r^P(^3CT \rightarrow S_0)$ is 2.48 × 10^3 s^{-1} and $k_{r,avg}$ increases by an order of magnitude to 1.24 × 10^4 s^{-1}. Interestingly, there is a low frequency mode (ν_{16} ~ 168 cm^{-1}) that involves the elongations of Au–C(phenyl-DPA) and C(phenyl)–N(DPA) distances; thus we have also computed the k_r and ΔE_{ST} with this thermally accessible ν_{16} distortion (**7-distorted**). The ΔE_{ST} decreases to ~1200 cm^{-1} with $k_r^P(^3CT \rightarrow S_0)$ increased to 4.95 × 10^3 s^{-1}. More importantly, the $k_{r,avg}$ becomes 1.15 × 10^5 s^{-1}. Hence, TADF is much more efficient in **7**. Compared with the experimental k_r of **7**, which is also of the order 10^5 s^{-1}, the much faster k_r of **7**, as compared with **3**, is due to the much enhanced TADF efficiency in the former complex because the placement of the DPA at the phenyl ring *trans* to the pyridine ring allows better separation of the HOMO and LUMO and hence a smaller ΔE_{ST}.

Organic-Light Emitting Devices

Vacuum-deposited OLEDs based on **4**, **7** and **8** were fabricated

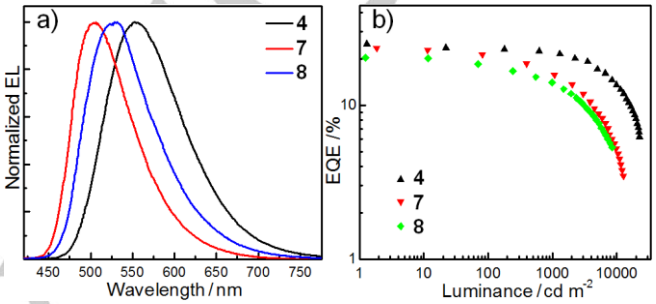

Figure 6. a) Normalized EL spectra and b) EQE-luminance characteristics of OLEDs based on **4** (16 wt%), **7** (8 wt%) and **8** (4 wt%).

. External quantum efficiency (EQE) versus luminance characteristics of the optimized **4**, **7** and **8** devices are depicted in Figure 6b and key EL performances of **4** are summarized in Table 3. These Au^{III}-TADF emitters realize maximum EQEs of over 20 % (23 % and 20 % of the device with 4 wt% **7** and 4 wt% **8** respectively). Both maximum EQE and efficiency roll-off of the device with 16 wt% **4** were superior to those of the other devices, owing to its higher Φ and shorter τ in thin films as described in Table 1. Maximum EQE of 25.03 %, CE of 77.78 cd A^{-1} and PE of 94.00 lm W^{-1} were achieved in the device with 16 wt% **4**. Notably, a high EQE of 22.01 % was maintained at a high luminance of 1000 cd m^{-2}. Such performance is among the best of reported Au^{III}-OLEDs and comparable to that of Au^{I}-OLEDs (Table S17).[1a,b,d,e] The operational lifetime of OLED prepared with **4** has been measured under our laboratory conditions and compared with that of the best pincer Au(III)-acetylide TADF emitter from our previous report[1e] under the same device configuration (Table S18). The OLED of **4** exhibited operational lifetime LT_{95} of 1.97 h at initial luminance of 10390 cd m^{-2}, corresponding to 105 h at 1000 cd m^{-2} and 5280 h at 100 cd m^{-2}, which are the best among all reported Au(III)-OLEDs.

Discussion

With a view to developing robust and strongly emissive Au^{III} complexes for practical material applications, we conceive that the research on Au^{III} complexes supported by tetradentate ligands having C-donor atoms is critical yet far less explored.

Tetradentate Au^{III} complexes supported by confused porphyrin and corrole have been reported to be emissive, but they exhibit NIR phosphorescence with low quantum yields and long emission lifetimes.[9] In 2017, Yam et al. reported N-bridged tetradentate Au^{III} complexes.[3d] By connecting the bound tridentate C^N^C and monodentate acetylide ligand via an amino linkage, tetradentate Au^{III} complexes having a 12-membered metallocycle have been furnished. These complexes exhibit phosphorescence with Φ of 0.41-0.49 and τ of 5.3-10.8 μs in deaerated CH_2Cl_2 at room temperature. However, due to the presence of amino linker in the ligand, their emissive excited states are confined to ^{3}ILCT ones, which results in a narrow emission maxima range of 584-615 nm, posing a constraint on the tuning of photophysical and excited state properties.

In this work, an aryloxy-substituted C^N^C ligand serves as the core tetradentate C^C^N^C ligand scaffold for complexes **1**-**8**. A major hurdle in the preparation of these complexes is the difficulty in forming the third metallocycle. Traditional synthesis via conventional heating has been attempted but failed to give the desired product. In light of the successful preparation of [Au(C^C^N)] complexes via the use of microwave irradiation,[5c,e] we then sought to achieve the last cyclometalation step with this method which was found to give the expected tetradentate Au^{III} complexes in high yields (90 %). Regarding the design of the ligand, the placement of the aryloxy-substituent on the 3-position of the phenyl ring of C^N^C moiety allows the formation of 5-5-6 membered chelate rings which may confer higher structural rigidity for minimizing k_{nr}. Furthermore, since the aryloxy-related excited state would be higher-lying than that arising from amino-substituents, it allows post-synthetic installation of different amino-substituents on the C^C^N^C scaffold for tuning the emission color over a wide range. For **9**, instead of an O-bridge, a spiro-fluorene has been employed to link pyridine and phenyl for forming a 6-membered metallocycle. Unlike the O-bridged complexes, this spiro-fluorene-bridged complex could only be prepared via successive microwave-assisted C-H activation. Although **9** is also supported by a C^C^N^C ligand, it is unexpectedly very weakly emissive (Φ = 0.003, in toluene). One possible reason is the facile motion of its spiro-fluorene unit in solution, as reflected by the ^{1}H NMR spectra of **9** in deuterated toluene at room temperature and at -60 ^{o}C both showing that the two *t*Bu groups on the spiro moiety give identical signal (a singlet; note the different environments of the two *t*Bu groups in the crystal structure of **9** depicted in Figure 2).

The O-bridged tetradentate ligand system described herein is highly versatile, affording Au^{III} complexes exhibiting long-lived ^{3}IL emissive excited states with Φ of up to 0.54 and τ of up to 225 μs in degassed solution at room temperature, and also complexes showing TADF with Φ of up to 0.94 and τ < 2 μs via the addition of amino-substituent on the ligand. The Φ of 0.94 shown by **7** is the highest value among luminescent Au^{III} complexes.[10] In contrast to N-bridged tetradentate Au^{III} complexes, the emission color of these O-bridged Au^{III} complexes is highly tunable and spans from blue-green (485 nm) to red (612 nm). It is interesting to note that although the amino-substituted aryl moiety in complexes **7** and **8** is linked by an O-bridge which may limit the rotation and dihedral angle of the aryl moiety, these two complexes still exhibit efficient TADF similar to the tridentate counterparts.[1a]

Emitters having high Φ and short τ are ideal for realizing OLEDs with high EQE and small efficiency roll-off. Vacuum-deposited OLEDs based on Au^{III}-TADF emitters **4**, **7** and **8** all showed excellent performance with maximum EQE over 20 %, comparable to the best ones based on tridentate Au^{III} emitters[1a,d,e] and significantly higher than OLEDs with N-bridged tetradentate Au^{III} emitters (maximum EQE = 11.1 %).[3d] The OLED fabricated with 16 wt% of **4** is the best performing one, with EQE of 22.01 % at a practical luminance of 1000 cd m^{-2}.[1e] The high Φ (0.89) and short τ (1.69 μs) of **4** in thin film are the critical factors accounting for the high efficiency at high brightness. In our previous study, the operational lifetime of the device fabricated with tridentate gold(III) TADF emitter[1e], as evaluated by Samsung, was the best for Au(III)-OLEDs[1d]. In this work, the device data evaluated under our laboratory conditions revealed that the device with **4** showed a LT_{95} of 5280 hours at 100 cd m^{-2}, which is more than 10 times better than those achieved with tridentate emitters. This finding signifies the importance of employing tetradentate ligand scaffold in the design of stable and structurally robust Au(III)-TADF emitters for practical applications.

Conclusion

In summary, charge-neutral, cyclometalated tetradentate Au^{III} complexes with trianionic O-bridged/spiro-arranged C^C^N^C ligands have been successfully synthesized through microwave-induced reactions. By modifying the nature and positions of substituents, these tetradentate Au^{III} complexes display strong photoluminescence originating from three different kinds of emission origins (^{3}IL, ^{3}ILCT and TADF) with Φ of up to 0.94 in degassed toluene. Temperature-dependent emission studies and DFT/TDDFT calculations both support that the emission mechanism of complexes with large k_r and short τ involves TADF. Ultrafast time-resolved spectroscopic measurements conducted on these tetradentate Au^{III} complexes revealed τ_{ISC} of 0.4−56 ps and estimated k_{ISC} of 0.2−25 $\times$ 10^{11} s^{-1}. Vacuum-deposited OLEDs fabricated with these tetradentate Au^{III}-TADF emitters showed excellent performance with maximum EQEs of up to 25 %, and EQEs of up to 22 % at a luminance of 1000 cd m^{-2}. The findings in this work underpin the competitiveness of Au^{III}-TADF emitters among phosphorescent Ir^{III} and Pt^{II} emitters for OLED application. It is envisaged that this type of Au^{III} complexes would serve as a robust and versatile class of material which will excel in diverse applications.

Acknowledgements

This work was supported by the Basic Research Program of Shenzhen (JCYJ20160229123546997, JCYJ20170818141858021 and JCYJ20180508162429786), Hong Kong Research Grants Council (HKU 17330416), CAS-Croucher Funding Scheme for Joint Laboratories, the Major Program of Guangdong Basic and Applied Research (2019B030302009) and the National Key Basic Research Program of China (2013CB834802). This work was also conducted in part using the research computing facilities and/or advisory services offered by Information Technology Services, The University of Hong Kong. We thank Dr. K.-H. Low for assistance in solving the X-ray crystal structures of **1**, **5** and **9**.

Keywords: gold • TADF • tetradentate • microwave • OLED

[1] a) W.-P. To, D. Zhou, G. S. M. Tong, G. Cheng, C. Yang, C.-M. Che, *Angew. Chem. Int. Ed.* **2017**, *56*, 14036-14041; *Angew. Chem.* **2017**, *129*, 14224-14229; b) D. Di, A. S. Romanov, L. Yang, J. M. Richter, J. P. H. Rivett, S. Jones, T. H. Thomas, M. A. Jalebi, R. H. Friend, M. Linnolahti, M. Bochmann, D. Credgington, *Science* **2017**, *356*, 159-163; c) P. J. Conaghan, S. M. Menke, A. S. Romanov, S. T. E. Jones, A. J. Pearson, E. W. Evans, M. Bochmann, N. C. Greenham, D. Credgington, *Adv. Mater.* **2018**, *30*, 1802285; d) L.-K. Li, M.-C. Tang, S.-L. Lai, M. Ng, W.-K. Kwok, M.-Y. Chan, V. W.-W. Yam, *Nat. Photonics* **2019**, *13*, 185-191; e) D. Zhou, W.-P. To, Y. Kwak, Y. Kwak, Y. Cho, G. Cheng, G. S. M. Tong, C.-M. Che, *Adv. Sci.* **2019**, *6*, 1802297.

[2] a) D. A. K. Vezzu, J. C. Deaton, J. S. Jones, L. Bartolotti, C. F. Harris, A. P. Marchetti, M. Kondakova, R. D. Pike, S. Huo, *Inorg. Chem.* **2010**, *49*, 5107-5119; b) S. C. F. Kui, P. K. Chow, G. S. M. Tong, S.-L. Lai, G. Cheng, C.-C. Kwok, K.-H. Low, M. Y. Ko, C.-M. Che, *Chem. Eur. J.* **2013**, *19*, 69-73; c) G. Cheng, P.-K. Chow, S. C. F. Kui, C.-C. Kwok, C.-M. Che, *Adv. Mater.* **2013**, *25*, 6765-6770; d) S. C. F. Kui, P. K. Chow, G. Cheng, C.-C. Kwok, C. L. Kwong, K.-H. Low, C.-M. Che, *Chem. Commun.* **2013**, *49*, 1497-1499; e) G. Cheng, S. C. F. Kui, W.-H. Ang, M.-Y. Ko, P.-K. Chow, C.-L. Kwong, C.-C. Kwok, C. Ma, X. Guan, K.-H. Low, S.-J. Su, C.-M. Che, *Chem. Sci.* **2014**, *5*, 4819-4830; f) T. Fleetham, G. Li, L. Wen, J. Li, *Adv. Mater.* **2014**, *26*, 7116-7121; g) K.-Y. Liao, C.-W. Hsu, Y. Chi, M.-K. Hsu, S.-W. Wu, C.-H. Chang, S.-H. Liu, G.-H. Lee, P.-T. Chou, Y. Hu, N. Robertson, *Inorg. Chem.* **2015**, *54*, 4029-4038; h) P.-K. Chow, G. Cheng, G. S. M. Tong, C. Ma, W.-M. Kwok, W.-H. Ang, C. Y.-S. Chung, C. Yang, F. Wang, C.-M. Che, *Chem. Sci.* **2016**, *7*, 6083-6098; i) T. Fleetham, Y. Ji, L. Huang, T. S. Fleetham, J. Li, *Chem. Sci.* **2017**, *8*, 7983–7990; j) G. Li, A. Wolfe, J. Brooks, Z.-Q. Zhu, J. Li, *Inorg. Chem.* **2017**, *56*, 8244-8256; k) L. Liu, X. Wang, N. Wang, T. Peng, S. Wang, *Angew. Chem. Int. Ed.* **2017**, *56*, 9160-9164; *Angew. Chem.* **2017**, *129*, 9288-9292; l) Z.-Q. Zhu, C.-D. Park, K. Klimes, J. Li, *Adv. Opt. Mater.* **2019**, *7*, 1801518.

[3] a) G. Cheng, K. T. Chan, W.-P. To, C.-M. Che, *Adv. Mater.* **2014**, *26*, 2540-2546; b) K. T. Chan, G. S. M. Tong, Q. Wan, G. Cheng, C. Yang, C.-M. Che, *Chem. Asian J.* **2017**, *12*, 2104-2120; c) M.-C. Tang, C.-H. Lee, S.-L. Lai, M. Ng, M.-Y. Chan, V. W.-W. Yam, *J. Am. Chem. Soc.* **2017**, *139*, 9341-9349; d) B. Y.-W. Wong, H.-L. Wong, Y.-C. Wong, M.-Y. Chan, V. W.-W. Yam, *Angew. Chem. Int. Ed.* **2017**, *56*, 302-305; *Angew. Chem.* **2017**, *129*, 308-311; e) M.-C. Tang, W.-K. Kwok, S.-L. Lai, W.-L. Cheung, M.-Y. Chan, V. W.-W. Yam, *Chem. Sci.* **2019**, *10*, 594-605.

[4] M. Saigo, K. Miyata, S. Tanaka, H. Nakanotani, C. Adachi, K. Onda, *J. Phys. Chem. Lett.* **2019**, *10*, 2475-2480.

[5] a) A. P. Shaw, M. Tilset, R. H. Heyn, S. Jakobsen, *J. Coord. Chem.* **2011**, *64*, 38-47; b) E. Langseth, C. H. Gorbitz, R. H. Heyn, M. Tilset, *Organometallics* **2012**, *31*, 6567-6571; c) R. Kumar, A. Linden, C. Nevado, *Angew. Chem. Int. Ed.* **2015**, *54*, 14287-14290; *Angew. Chem.* **2015**, *127*, 14495-14498; d) T. von Arx, A. Szentkuti, T. N. Zehnder, O. Blacque, K. Venkatesan, *J. Mater. Chem. C* **2017**, *5*, 3765-3769; e) M. S. M. Holmsen, A. Nova, K. Hylland, D. S. Wragg, S. Oien-Odegaard, R. H. Heyn, M. Tilset, *Chem. Commun.* **2018**, *54*, 11104-11107.

[6] A. P. Monkman in H. Yersin, Ed. Highly Efficient OLEDs-Materials Based on Thermally Activated Delayed Fluorescence. *Wiley-VCH*: Weinheim, Germany, **2019**, p. 425-463.

[7] a) F. I. Mopsik, *J. Chem. Phys.* **1969**, *50*, 2559-2569; b) M. Aydemir, S. Xu, C. Chen, M. R. Bryce, Z. Chi, A. P. Monkman, *J. Phys. Chem. C* **2017**, *121*, 17764-17772.

[8] a) W.-P. To, K. T. Chan, G. S. M. Tong, C. Ma, W.-M. Kwok, X. Guan, K.-H. Low, C.-M. Che, *Angew. Chem. Int. Ed.* **2013**, *52*, 6648-6652; *Angew. Chem.* **2013**, *125*, 6780-6784; b) K. T. Chan, G. S. M. Tong, W.-P. To, C. Yang, L. Du, D. L. Phillips, C.-M. Che, *Chem. Sci.* **2017**, *8*, 2352-2364.

[9] a) M. Toganoh, T. Niino, H. Furuta, *Chem. Commun.* **2008**, 4070-4072; b) M. Soll, K. Sudhakar, N. Fridman, A. Müller, B. Röder, Z. Gross, *Org. Lett.* **2016**, *18*, 5840-5843; c) A. B. Alemayehu, N. U. Day, T. Mani, A. B. Rudine, K. E. Thomas, O. A. Gederaas, S. A. Vinogradov, C. C. Wamser, A. Ghosh, *ACS Appl. Mater. Interfaces* **2016**, *8*, 18935-18942; d) C. M. Lemon, D. C. Powers, P. J. Brothers, D. G. Nocera, *Inorg. Chem.* **2017**, *56*, 10991-10997.

[10] a) J. M. López-de-Luzuriaga, M. Monge, M. E. Olmos, *Dalton Trans.* **2017**, *46*, 2046-2067; b) R. Kumar, C. Nevado, *Angew. Chem. Int. Ed.* **2017**, *56*, 1994-2015; *Angew. Chem.* **2017**, *129*, 2024-2046.